

Determination of high-frequency wind variability from observations and application to North Atlantic wave modeling

Eva Bauer

Potsdam-Institut für Klimafolgenforschung, Potsdam, Germany.

Ralf Weisse

GKSS Forschungszentrum, Institut für Gewässerphysik, Geesthacht, Germany.

J. Geophys. Res., 105(C11), 26,179-26,190, 2000

Abstract

The influence of quasi-realistic high-frequency wind variability for the probability distribution of surface waves and for the skill of the predictions with the wave model WAM is investigated. So far, the sensitivity of the surface wave field to high-frequency wind variability has been demonstrated only for idealized wave conditions or particular events using rather simplified high-frequency wind forcings. In this study the problem is addressed more generally by estimating the high-frequency wind variability (for periods shorter than 6 hours) and by assessing its relevance for a particular North Atlantic winter. Wind observations with 20 minute time resolution are used to build a statistical wind generator which reconstructs (in a statistical sense) that fraction of the wind variability that is missing in the analyzed model wind fields. These quasi-realistic wind fluctuations, superimposed on analyzed 6 hourly wind fields, produced an increase of the air-sea momentum flux and resulted in a moderate but systematic increase of the average wave heights and in their short-term variability. While the results are qualitatively consistent with the findings of earlier studies under simplified conditions they differ quantitatively. The change of the distribution of the wave data is found to be less pronounced for young sea states in the storm track region than for older sea states in the low latitudes. The response yields everywhere a significant amplification of the spectral variance for periods below 12 hours and an increase of the probability of extreme wave heights. Thus, the increased air-sea momentum flux is seen to be effective for predictions of the probability distribution of wave data and may also influence predictions of the ocean circulation.

1. Introduction

Short-term predictions of global atmospheric wind and ocean surface wave fields are now in common use for shipping and off-shore industry. Weather centers provide routine global predictions with atmospheric models already since about the 1970s, while the routine global ocean wave prediction has established only since about 1990. Wave predictions are obtained from wave models which are forced by analyzed or predicted near-surface winds from atmospheric models. At the beginning global wave models had a horizontal resolution of the order of 300 km and the driving wind fields were supplied with a similar spatial resolution at time intervals of 6 hours. To account for the shorter time step of the wave model the wind is often linearly interpolated in time between two consecutive driving wind fields.

Within the last few years the physics and the numerics of both the atmosphere and the wave models were developed further by exploiting the growing information from in situ data and satellite observations. At the same time computational resources have improved considerably. As a result, global wave predictions nowadays have a horizontal resolution of typically 50 km. For regional or local wave model studies even much finer horizontal resolutions are used [e.g., Schneggenburger *et al.*, 1997]. However, the time interval at which the driving wind fields are supplied to the wave models (usually 6 hours) remained unchanged until today. This rather coarse temporal resolution is directly related to the conventional output interval of atmospheric models, the global synoptic network system, and the conventional data assimilation schemes used.

The third-generation wave model WAM [WAMDI Group, 1988] has become one of the standard tools for global wave predictions. On average the absolute values of the modeled wave data compare well with global observations. Sometimes, however, large deviations of both signs between instantaneous values from modeling and observation are reported [e.g., Sterl *et al.*, 1998; Heimbach *et al.*, 1998]. Since the quality of the wave prediction depends crucially on the quality of the driving wind fields, for two reasons the question arises whether the coarse temporal resolution of 6 hours of the driving wind fields might be disadvantageous for wave predictions: First, the physical response time of wind-generated waves to the wind force is clearly less than 6 hours. Wind waves evolve instantaneously according to resonance conditions with the winds in the atmospheric boundary layer [Miles, 1957]. In practice, the wind fields are kept constant for 6 hours or they are interpolated linearly in time during the integration of the wave model. Thereby, the natural high-frequency

wind variability with time scales of less than 6 hours is suppressed almost completely. So, the corresponding response of the wave model to wind fluctuations, which are mainly associated with baroclinic instabilities and with the passage of atmospheric fronts, is missing.

Second, it is often suggested that the underestimation of the short-scale variability may involve underestimations also of variabilities on other scales. Variance spectra of observed wind speeds and significant wave heights (SWH) are characterized by similar spectral slopes. This was demonstrated for wavenumber spectra over a wide range of horizontal scales [e.g., *Monaldo*, 1990; *Tournadre et al.*, 1996; *Bauer*, 1997]. While for large to medium spatial scales the wind and SWH spectra correspond closely to those obtained from modeled data, this correspondence applies not for the smaller spatial scales. In particular, for scales smaller than 500 km the wind speed spectrum and the SWH spectrum obtained from modeled data underestimate the variance of the observed spectra considerably [e.g., *Tournadre et al.*, 1996; *Bauer*, 1997]. Similar results were found for the frequency spectra of modeled and observed wind speed and SWH (as shown below). As an initial step, it is considered useful to investigate in which manner the high-frequency variability of SWH is changed through increased high-frequency wind variability.

A number of numerical studies investigated the impact of simplified high-frequency wind fluctuations on the wave field under idealized conditions. It was shown that additional wind variability results not only in an increase of the SWH variance but also in an increase of the mean wave height. For instance, *Cavaleri and Burgers* [1992] forced a one grid point version of the wave model WAM with a wind of constant speed and superimposed random Gaussian-distributed high-frequency wind fluctuations. They found that with increasing variance and with increasing duration (or correlation in time) of the random wind speed fluctuations the growth curve of SWH diverges increasingly from that of constant winds. For instance, using a constant wind speed of 18.45 m s^{-1} and superimposing Gaussian wind speed fluctuations with a variance of 30% relative to the (constant) mean wind speed an increase of 30% of the SWH at full development was found. *Cavaleri and Burgers* [1992] showed that these differences could primarily be attributed to an asymmetry of the wind input source function with respect to the excess of wind speed over the phase speed of the waves. To transfer energy from the wind to the waves the wind speed has to be larger than the phase speed of the waves. Therefore, even if the high-frequency wind speed fluctuations average out over a longer time period, positive wind fluctuations always enhance the wave growth while negative

wind fluctuations produce less wave growth on average or eventually no wave growth if the wind speed drops below the phase speed of the existing waves.

The potential importance of high-frequency wind variability was also demonstrated for two-dimensional realistic model domains and realistic wind fields [e.g., Cavaleri, 1994; Ponce and Ocampo-Torres, 1998]. However, in these studies again idealized wind fluctuations with exaggerated noise levels were applied. So far, no study has been performed in which the impact of quasi-realistically derived wind fluctuations on wave prediction and wave probability distributions was investigated. Therefore, in this study a statistical generator for quasi-realistic wind fluctuations is derived from high-resolution and high-quality wind measurements [Tournadre, 1993] taken at the oil platform Frigg in the northern North Sea. The generator is capable of producing non-Gaussian wind speed fluctuations with periods less than 6 hours in agreement with the high-frequency wind fluctuations contained in observations. Subsequently, a set of experiments with the wave model WAM is performed in which the model is forced with analyzed 6 hourly wind fields with and without superimposed high-frequency wind fluctuations.

The WAM model integrations are carried out for the winter season in the North Atlantic. In this region the natural high-frequency wind variability associated with baroclinic instabilities is large and the wave height variability is worldwide the largest. This can be inferred from the frequency distribution of the observed SWH which is characterized by the largest range and the largest extreme wave heights in the North Atlantic [e.g., Bauer and Staabs, 1998]. Moreover, the sea-going activities are manifold in the North Atlantic and reliable predictions of the mean and the fluctuations around the mean are of large interest.

The study is structured as follows. In section 2 we present the generator for the high-frequency wind fluctuations. In section 3 we briefly describe the wave model WAM and the experiments performed. Our results are presented in section 4 and a summary with discussion is given in section 5.

2. A generator for high-frequency wind fluctuations

2.1. Orthogonal decomposition of the fluctuations

Usually wave models are forced with analyzed winds which are available only every 6 hours. Between two analysis times the wind is either kept constant or is interpolated linearly in time thereby underestimating the wind variability related to various high-frequency meteorological

events such as the passage of atmospheric fronts and the associated gustiness. The following statistical approach represents a scheme to upgrade the conventional 6 hourly analyzed wind fields through adding quasi-realistic high-frequency wind fluctuations.

Let us denote a time series of wind speed observations taken every 20 minutes by y_t where the index $t = 1 \dots N$ represents the time and N the number of observations. From this time series a new time series y_l may be derived by sub-sampling the original time series every 6 hours. From the sub-sampled time series again a 20 min time series may be obtained by linear interpolation. The original time series y_t can then be written as

$$y_{n(l-1)+s} = y_{n(l-1)+1} + \frac{y_{nl+1} - y_{n(l-1)+1}}{n}(s-1) + x_{n(l-1)+s} \quad (1)$$

Here $s = 1 \dots n$ denotes the time index of the observations within a 6 hour period (the ‘‘short-term’’ fluctuations), n the number of observations within this period and $l = 1 \dots Nn^{-1}$ the time index of the observations sampled every 6 hours (the ‘‘long-term’’ fluctuations). Thus, the first two terms on the r.h.s. of (1) represent the 6 hourly instantaneous wind and the linearly interpolated wind between two consecutive 6 hour wind fields. Usually, only the first term or the first two terms on the r.h.s. of (1) are used to drive a wave model. For our purposes, we assume that the first two terms are known exactly. The last term $x_{n(l-1)+s}$ on the r.h.s. of (1) represents the high-frequency wind fluctuations (or the error) we want to model statistically.

For simplicity of notation let \mathcal{X} denote the $n \times Nn^{-1}$ matrix of the fluctuations which has the ‘‘short-term’’ fluctuations in its rows and the ‘‘long-term’’ fluctuations in its columns

$$\mathcal{X} = (x_{sl}) \quad (2)$$

where $x_{sl} = x_{n(l-1)+s}$. From (1) follows for $s = 1$ that $(x_{1l}) = 0$ which reduces the dimension of the problem to $(n-1) \times Nn^{-1}$. In the following \mathcal{X} therefore refers to the $(n-1) \times Nn^{-1}$ matrix (x_{sl}) with $s = 2 \dots n$. In order to obtain consistent wind speed fluctuations from a random number generator we are seeking for a decomposition

$$\mathcal{X} = \mathcal{P}\tilde{\epsilon} \quad (3)$$

such that the covariance

$$\mathcal{C} = \frac{n}{N}\mathcal{X}\mathcal{X}^T \quad (4)$$

of the fluctuations within a 6 hour period is retained. One possible decomposition which fulfills this condition is the representation by Empirical Orthogonal Functions (EOF)

[e.g., von Storch and Zwiers, 1999]. In this case \mathcal{P} is the $(n-1) \times (n-1)$ matrix which has the EOFs in its columns, and $\vec{\epsilon}$ is the $(n-1)$ -dimensional column vector of the EOF coefficients for the $(n-1)$ EOF patterns. In our case the EOFs represent the correlated wind fluctuations within a 6 hour period and the EOF coefficients describe the sequence of such intervals. In the next section we show that the model represents the observed conditions reasonably and how the EOF coefficients can be modeled with the help of a Gaussian white noise process.

2.2. Fitting and verification of the wind generator

The proposed statistical model was fitted using wind speed measurements taken every 20 minutes for the two years 1983 and 1984. The observations [Tournadre, 1993] were taken at the oil platform Frigg in the northern North Sea (60° N, 2° E). The measurements were sub-sampled every 6 hours and the sub-sample was then interpolated linearly onto 20 min time steps yielding the first two terms on the r.h.s of (1). Subsequently, the high-frequency wind fluctuations (x_{st}) were obtained by subtracting the interpolated time series from the original time series.

The covariance matrix of the high-frequency wind fluctuations (x_{st}) indicates that these fluctuations do not represent a white noise process. Although covariances are largest in the principal diagonal of the matrix, the non-diagonal elements have smaller but non-zero values (not shown). In our case, each covariance in the principal diagonal represents the covariance of all high-frequency wind fluctuations taken at a particular time within the 6 hour time slots, while the non-diagonal elements represent the cross-covariances between fluctuations at different times within the 6 hour time slots. The latter provide a measure of the decorrelation time of the high-frequency wind fluctuations and would be zero if the high-frequency fluctuations could be considered as white noise. Further, within the principal diagonal the covariances are not constant. Instead, they are largest in the middle of a 6 hour period which means that on average the deviations of the instantaneous winds from the interpolated winds grow with time-distance from those times at which the 6 hourly instantaneous values were sub-sampled. At the sub-sampling times the winds of the interpolated time series correspond to the original winds and the deviations are zero per definition.

The basic structure of the covariance matrix is reflected by the first EOF pattern (Figure 1a) which describes almost 55% of the total variance. The structure of the fluctuations between consecutive 6 hour intervals is represented by the EOF coefficients. In contrast to the short-term fluctuations within a 6 hour slot, the long-term fluctuations

of consecutive 6 hour intervals are found to be uncorrelated (Figure 1b). This holds for the EOF coefficients of all EOF patterns. However, a closer inspection reveals that the EOF coefficients are not Gaussian distributed. In order to obtain Gaussian distributed fluctuations that may be generated with a Gaussian random number generator we used the so-called probability integral (probit) transformation [e.g., Bürger, 1996]

$$\epsilon_t^* = \Phi^{-1}(F(\epsilon_t)) \quad (5)$$

Here F denotes the empirical cumulative distribution function (CDF) of the EOF coefficients and Φ the CDF of the standard normal distribution. To minimize the number of free parameters a joint empirical CDF for all EOF coefficients was estimated. Figure 1c shows the quantiles of the standard normal and of the probit-transformed coefficient time series of the first EOF. It can be inferred that both distributions can not be separated at the 99% confidence level. This permits to use a Gaussian random number generator in conjunction with the backward transformation of (5) to obtain quasi-realistic samples of the EOF coefficient time series.

The generator for quasi-realistic high-frequency wind fluctuations consists of two components, a turbulent component and a stochastic component. The turbulent component describes the statistical properties of fluctuations with time scales shorter than 6 hours which obey the ordering prescribed by the EOF patterns. The stochastic component describes the statistical properties of the sequence of EOF patterns, i.e. the properties of the fluctuations for periods longer than 6 hours. The latter are random but non-Gaussian distributed.

Technically, the wind generator is composed of 4 constituents: (i) Gaussian distributed random numbers ϵ_t^* with zero mean and unit standard deviation are generated by a standard random number generator; (ii) the random numbers are probit-transformed to be compatible with the frequency distribution of the EOF coefficients estimated from observations using the backward transformation (5); (iii) each EOF is multiplied with a transformed random number (3) to obtain time series of 20 min wind speed fluctuations for a 6 hour interval; (iv) the time series of fluctuations are then superimposed onto the driving wind fields which were interpolated to the integration time step (20 minutes) using (1). At Frigg the application of this scheme increases the variance of the analyzed wind fields by about 8% compared to the variance of the interpolated wind speed time series.

The skill of the proposed generator for high-frequency wind fluctuations is tested using an independent sample of temporal high-resolution wind speed data at the oil plat-

form Ekofisk (56.5° N, 3.2° E) for 1996. We compared the measured wind speed spectrum with the spectrum obtained from sub-sampling and interpolating the Ekofisk time series as well as with the spectrum from superimposing the wind fluctuations of our wind generator (Figure 2). The spectrum of the original measurements taken every 20 minutes is regarded to represent the magnitude and the slope of the natural spectral variance. For periods longer than 6 hours all spectra overlap within the 95% confidence interval. However, for periods less than 6 hours the spectrum of the linearly interpolated time series clearly underestimates the natural variance as a result of the low-pass filtering of the sub-sampling procedure. By the application of the high-frequency wind generator the natural variance spectrum is recovered within the error bounds. Thus the superimposed wind fluctuations are capable of filling up the missing fraction of the high-frequency variance in the interpolated time series.

3. Setup of the WAM model experiments

The numerical experiments were performed with the wave model WAM cycle 4 [Komen *et al.*, 1994]. The WAM model integrates the wave transport equation using an explicit advection scheme and an implicit scheme for the wave source functions. The source functions consist of the wind input function, the nonlinear wave-wave interaction function [Hasselmann and Hasselmann, 1985; Hasselmann *et al.*, 1985] and the dissipation function [Hasselmann, 1974]. The wind input source function describes the turbulent momentum transfer between the atmospheric boundary layer flow and the sea surface waves using the theory of Janssen [1989]. In this theory the parameterization of the wave growth is based on the quasi-laminar theory of Miles [1957] which yields an exponential wave growth. The three source functions are balanced such that the modeled wave growth curves agree best with observed wave growth curves from ideal fetch-limited and duration-limited situations with steady winds. The growth curves describe the changes of the normalized wave energy and wave frequency as a function of essentially two variables, i.e. the fetch and the wind duration [e.g., Komen *et al.*, 1994]. To account also for the wave-induced air-sea momentum flux the wind input source function was extended by a second-order term describing the coupling between the atmospheric flow and the surface waves [Janssen, 1989; 1991]. The wave-induced flux depends nonlinearly on the wave energy spectrum and implicitly on the wave age and is highly sensitive to changing winds.

In our experiments the WAM model was forced with analyzed winds obtained from the ECMWF re-analysis

project with a horizontal resolution of T106 [Gibson *et al.*, 1996]. We used the diagnostically derived 6-hour wind fields at 10 m height above the sea surface which are henceforth called u_{10} winds. The model domain covers the North Atlantic area from 19°N to 70°N and from 82°W to 20°E with a spatial resolution of $1^\circ \times 1^\circ$. The wave energy is integrated in the direction-frequency domain which is discretized by 24 directional bins yielding a resolution of 15° , and 25 frequency bins with a logarithmic spacing between 0.04 and 0.41 Hz. For the integration a time step of 20 minutes was used to fulfill the numerical stability criterion and to correspond to the time resolution of the wind observations at Frigg and Ekofisk. At selected locations the model results were stored every time step and a complete model output was stored every 6 hours.

Three experiments were performed for the half-year period from 1 October 1983 until 31 March 1984: In the control run (CTR) the analyzed 6 hourly u_{10} winds were used with linearly interpolated winds between two analysis times. In the first sensitivity experiment (HF1) the model was driven by the winds of the CTR run but with added high-frequency wind fluctuations from our wind generator. Then the response of the model to higher noise levels was investigated in a second sensitivity experiment (HF3). The HF3 experiment is essentially identical with the HF1 experiment but the amplitude of the high-frequency wind speed fluctuations was tripled.

In all experiments the high-frequency fluctuations were chosen independently at all grid points, i.e. there was no spatial correlation between the fluctuations. Although this is generally not the case it nevertheless represents a reasonable approximation for the present study: The high-frequency fluctuations at Frigg have typical decorrelation times of about 3 hours and correspondingly a rather short correlation length scale which is smaller than the coarse horizontal resolution (about 100 km) used in our experiments. Propagating signals are therefore damped out before they reach the next grid cell and the fluctuations can therefore be modeled independently at all grid points. For higher spatial resolutions the spatial correlation of the fluctuations has to be taken into account.

4. Impact of high-frequency wind fluctuations on North Atlantic waves

4.1. Comparison of statistical moments and frequency spectra of modeled and observed data at the Frigg location

The impact of the high-frequency wind fluctuations on the modeled wave field at the Frigg location was assessed by comparing the statistical moments of the probability

distributions of SWH and u_{10} from the three model experiments and the observations (Table 1). Compared to the observations the mean wind speed and the mean SWH are overestimated in all experiments. This offset seems to be caused by the location of the Frigg platform east of the Shetland Islands. At the given spatial resolution these islands are not resolved in the model grid and the “shadowing effect” from these islands on the observed wind speed and wave height at Frigg is not present in the model. Consequently, the mean wind speed and the mean SWH are larger in all model simulations compared to the observations. Because of this shortcoming the direct comparison of statistical moments from model and observation is limited.

The impact of the wind generator is assessed by the differences of the moments among the model experiments. They show, as expected, that the mean of the model wind speeds remained unchanged. The standard deviations of the winds of the HF1 and HF3 experiment are increased by 0.17 m s^{-1} and 0.51 m s^{-1} , respectively, compared to the control run. Compared to the CTR run the skewness of the wind speed distribution remained nearly unchanged in the HF1 experiment while in the HF3 experiment it shows a slight increase. This is in agreement with the statistical properties of the high-frequency wind fluctuations added in these experiments which had zero mean and non-zero standard deviation.

The increase in the wind speed variance at Frigg resulted in a moderate increase in the mean SWH by 0.1 m and 0.2 m in the HF1 and the HF3 experiment, respectively. This corresponds to an increase of approximately 3% and 6% in the sensitivity experiments with respect to the mean wave height of the control run. It is remarkable that the standard deviation of the SWH remained nearly unchanged in all three experiments while the skewness is slightly (with little statistical insignificance) enhanced in the sensitivity experiments indicating more extreme wave heights.

The impact of the wind generator is further seen in the frequency spectra of wind speeds and significant wave heights for periods less than about 12 hours. The capability of the wind generator to recover reasonably well the high-frequency wind variability was shown above for the Ekofisk data (Figure 2). The spectrum of the observed winds at the Frigg location also agrees well with the u_{10} spectrum of the HF1 experiment (not shown). In particular, there is no difference visible in the spectral level and in the slope between the spectra from the Frigg wind observations of 1983/1984 and from the Ekofisk wind observations of 1996. At both locations the high-frequency variability, which is underestimated in the wind fields of

the CTR experiment, is seen to be reliably recovered.

Although the total variance of the SWH remained nearly unchanged in the sensitivity experiments (Table 1) the variance at the high frequencies is clearly improved towards the observed spectrum (Figure 3a). The SWH spectrum from the observations is based on high-quality measurements with a radar distancemeter with 20 minutes resolution. Unfortunately, due to data gaps, the estimate of the observed SWH spectrum is based on a relatively short time series. Nonetheless, the spectrum shows the typical spectral slope of f^s with $s \approx -1.7$ within the 95% confidence interval. This slope was determined before by *Tournadre* [1993] and is about the same spectral slope as seen in the wind speed observations. In the CTR experiment the variance is up to 4 orders of magnitude smaller than in the observations for periods less than 24 hours. In the HF1 and HF3 experiment the high-frequency variance has grown by about one order of magnitude. However, the modeled spectra in the HF1 and the HF3 experiment are still too low and the spectral slope is too steep compared to the observed spectrum.

An interesting aspect of the wave model response is that the frequencies at which the strongest amplification of the variance occurs is different for wind speed than for SWH (Figure 3b,c). For the wind speed the amplification grows monotonically with decreasing period. The largest amplification occurs near the Nyquist frequency (40 minutes) with a factor of about 8 in the HF1 experiment and roughly 24 in the HF3 experiment while for periods longer than 12 hours the spectra remain nearly unchanged in both sensitivity experiments. The amplification of the SWH variance shows a distinct maximum at a period of roughly 3 hours in both sensitivity experiments and no amplification at the Nyquist frequency. The internal sensitivity of the modeled wave data appears to be too weak or the damping too strong to obtain a noticeable response at the highest frequency. At the period of 3 hours the SWH variance is amplified by about 30 in the HF1 experiment and by about 80 in the HF3 experiment. The downward shift of the frequency of largest amplification in the wave height spectrum is caused by the cumulative wave growth from the space-time integration of the wind forcing. This implies larger correlation scales in time for SWH than for wind speed. This is supported by observations which generally indicate that the dominant scales of variation in the wave data are slightly longer than in the wind data.

4.2. Changes in the probability distribution of the two dimensional fields of wave height and air-sea momentum flux

To investigate the changes in the probability distribution of the two dimensional wave height field we calculated the differences of the mean (Figure 4) and the ratio of the standard deviation of the SWH between the HF1 and the CTR experiment at each model grid point. The changes appear to be rather small but systematic: Compared to the CTR experiment the mean SWH is higher in the HF1 experiment everywhere in the North Atlantic. The SWH increase is in the order of 5 to 10 cm with the largest values found in the southern North Atlantic outside the storm track. Compared to the mean SWH in the CTR experiment these changes correspond to a relative increase in wave height of roughly 2% in the storm track and of 4 to 6% south of the storm track. South of approximately 35°N the standard deviation of the SWH is slightly enhanced in the HF1 experiment indicating a slightly broader probability distribution while there is almost no change in the standard deviation north of 35°N (not shown).

The variations in the local probability distributions of the SWH in our experiments are larger in the north-south direction while there are only minor changes in the east-west direction. We therefore summarize the changes for a region A, which is typical for the storm track, and region a B, which is typical for the conditions outside the storm track (Figure 4). For each region we calculated the differences of the quantiles of the probability distributions from two parameters describing the forcing (friction velocity and drag coefficient), from one parameter describing the wave-induced momentum flux (coupling ratio $R = \tau_w \tau^{-1}$ which is defined as the ratio between the wave-induced momentum flux (τ_w) and the total momentum flux (τ) at the air-sea interface) and from two parameters describing the wave response (SWH and mean frequency).

Although the mean wind speed u_{10} in the HF1 experiment remained unchanged compared to the control run, the probability distribution of the friction velocity u_* is shifted to larger values for all quantiles, i.e. at a given probability the friction velocity is larger in the HF1 experiment than in the CTR experiment (Figure 5a). This implies an enhanced air-sea momentum flux in the HF1 experiment compared to the control run. Additionally, the differences of the quantiles of the probability distribution of u_* tend to become larger with increasing probabilities which results in a broader and more skewed distribution in the HF1 experiment. The changes in the quantiles of u_* are similar within and outside the storm track, however, the magnitude of the changes is slightly larger outside the storm track.

The change in the probability distribution of the drag coefficient C_d is similar to the change in the frequency distribution of u_* . For a fixed probability the drag is generally larger in the HF1 experiment and the effect is larger outside the storm track (not shown). The similarity of the changes follows from the drag law which relates the drag coefficient $C_d(z)$ at height z to the wind speed $u(z)$ and the friction velocity u_*

$$u_* = \sqrt{C_d(z)}u(z). \quad (6)$$

Since the variability of the wind speed $u(z = 10\text{m})$ was enhanced but the mean remained unchanged the change of the probability distribution of u_* is closely connected to the changes of the probability distribution of C_d .

Changes of the coupling parameter R describe the changes of the wave-induced stress relative to the total stress. In the HF1 experiment the probability distribution of R broadens within and outside the North Atlantic storm track (Figure 5b). This indicates that both small and large values of R occurred more often. Primarily, this is related to higher (lower) wave-induced stresses for positive (negative) wind speed fluctuations. At the same time the simulations showed that the high-frequency wind speed fluctuations led on average to a reduced duration of the wind forcing and in turn to a reduced wave age which is usually associated with higher wave-induced stresses. The median of R is decreased in the HF1 experiment within the storm track while it is increased slightly outside the storm track. The variation of the median of R indicates that the changes of the wave-induced stress and of the total stress induced by the wind fluctuations and the shortening of the wind duration depends sensitively on the local conditions of the winds and the sea state.

The effects of the changed air-sea momentum flux on the SWH and the wave period are shown in Figure 5c and 5d, respectively. At a given probability the SWH is increased in the HF1 experiment and the entire probability distribution is shifted to larger values. Within the storm track this shift is about uniform while south of the storm track the offset increases with increasing probabilities which indicates a broader and more skewed probability distribution. In agreement with these changes the differences of the quantiles of the mean wave frequency between the HF1 and the CTR experiment are generally negative, indicating on average a lower mean wave frequency in the HF1 experiment. The impact in the HF3 experiment which was driven by tripled high-frequency wind variance is similar to the HF1 experiment but with enhanced changes in the air-sea momentum flux and in the wave response. Further explanations are presented in section 5.

4.3. Implications for the size of the potential error in wave predictions

An essential prerequisite for high quality wave predictions or wave hindcasts is the high quality of the driving wind fields. Sometimes, large deviations between observed and predicted wave heights occur which may at least partially be attributed to the quality of the wind forcing and/or the temporal resolution at which the wind forcing is supplied. The wind generator proposed in this study restores in a statistical sense that part of the missing variance in the driving wind fields that is due to the coarse temporal resolution of the wind input fields. Here restoring of the wind variance in a statistical sense means that is not possible with the wind generator to provide an exact estimate for an incorrect value at a given time. Nevertheless, an estimate of the order of magnitude of the error in wave height prediction that is caused by the coarse temporal resolution of the driving wind fields may be obtained in the following way: Let us suppose for the moment that the wind time series obtained from the driving wind fields plus the fluctuations from the wind generator represent the observed conditions exactly. In this case the influence of the coarse time resolution of the wind fields on the wave prediction can be obtained from the probability distribution of the instantaneous SWH differences between the HF1 and the CTR experiment (Figure 6). Again, the effect is largest south of the storm track. Here, an average error of 5% of the hindcast wave heights could be attributed to the missing variance in the driving wind fields. Within the storm track these potential errors are reduced to 2-3%. In 10% of the cases this effect is larger than 10% of the hindcast wave height and the absolute wave heights at particular times may differ by up to 1.4 m (not shown).

5. Summary and discussion

In wave model simulations the most common time interval at which driving wind fields are supplied is 6 hours. This time interval between consecutive wind analyses is directly related to the global synoptic network system and the conventional data assimilation schemes in use. As the horizontal resolutions of the wave model simulations became finer and finer in recent years, the time interval at which the wind fields were supplied to the wave models remained unchanged. This discretization in time represents a low-pass filter through which the wind variability with time scales less than 6 hours is suppressed completely. Thus high-frequency wind variability associated with baroclinic instabilities, the passage of atmospheric fronts and gustiness is strongly underestimated. Since surface waves are sensitive to this kind of wind forcing [e.g.,

Cavaleri and Burgers, 1992] modeled wave data lack the contributions of these high-frequency wind fluctuations. For instance, *Sterl et al. [1998]* forced a global version of the wave model WAM with the ECMWF re-analysis winds every 6 hours. They found that compared with observations the high wave heights were too small in their experiment and concluded that this was a result of underestimated extreme wind events in the high wind areas. These underestimations may be a result of both, the underestimation of the extreme wind speeds in the re-analysis itself and the coarse temporal resolution of the wind input fields.

In this study we assessed the response of the distribution of the wave data from the quasi-realistic high-frequency wind forcing during North Atlantic winter. We developed a statistical model which adapts the high-frequency variability of the driving wind fields to the high-frequency variability estimated from observations. The observed winds were taken from a two-year time series with a 20 min resolution at the oil platform Frigg. The wind generator was verified with an independent data set of wind speed observations from a different year taken at the oil platform Ekofisk. The proposed wind generator describes equally well the high-frequency variability of the wind speed at both platforms. This shows that the statistical properties of the high-frequency fluctuations obtained from our wind generator compare reasonably with observed fluctuations in the North Atlantic storm track. A limitation of the wind generator might arise from a missing verification with wind data outside the storm track where the mean wind speed is usually smaller. The high-frequency variance inserted in the analyzed model winds amounts to roughly 8% compared to the mean observed wind speed at Frigg and we assumed that the high-frequency wind variability is spatially independent. This implies that the relative contribution of the high-frequency wind variability from our wind generator is slightly, but negligibly, larger outside the storm track. However, the added variance produced at all locations wind speed spectra with the same continuous spectral decrease for increasing frequencies.

We run the wave model WAM with the 6-hour analyzed wind fields with and without additional wind speed fluctuations. The quasi-realistic perturbations of the wind fields produced everywhere in the North Atlantic a shift of the entire distribution of significant wave height to larger values. The relative changes of instantaneous SWH are estimated to be up to 15% but the mean of the SWH increased only by a few centimeters. The changes are found to be larger outside the North Atlantic storm track than within the storm track. Although the total wind vari-

ance increased significantly, the induced increase of the total SWH variance is negligible. Only for periods larger than 12 hours the spectral SWH variance increased significantly. While the maximum increase in the wind speed spectrum is at the highest resolvable frequency (corresponding to period of 40 minutes) the maximum increase in the SWH spectrum is shifted to a smaller frequency corresponding to 3 hours which is found independent of the amplitude of the high-frequency wind variance.

This work addressed a major source for inaccuracies in large scale wave modeling which is induced by underestimations of the high-frequency wind variance. Although our results showed that the mean wave response due to this error source is small we achieved a significant positive effect in the small scale variability of the wind and the wave data. The shift to lower frequencies of the maximum sensitivity of the SWH spectrum is attributed to the space-time integration of the wind forcing. This is in agreement with observations showing that the dominant scales of variation in the wave data are slightly longer than in the wind data.

The mean response of the wave model to the increased wind variability is induced by two opposing effects. The first effect is related to an asymmetry of the wind input source function with respect to the excess of wind speed over the phase speed of the waves [e.g., *Cavaleri and Burgers*, 1992; *Günther and Rosenthal*, 1995]. The findings of these studies are consistent with the results obtained here. The increase of the variance of the driving wind fields enhances the air-sea momentum flux and consequently enhances the wave growth. The effect accumulates with wind duration and is largest for saturated waves. The second effect is related to the reduced wind duration by increasing the wind variability. The reduction of the wind duration is seen everywhere in the model domain and leads to lower wave heights. The second effect is largest in duration-limited conditions.

The balance of both effects crucially influences the sign and the magnitude of the change of the SWH and may lead to different results depending on the properties of the wind fluctuations. In the present study the effect of increased air-sea momentum flux over-balances the effect of reduced wind duration. The mean response of the wave model is larger outside the storm track than within the storm track because in the mid latitudes of the North Atlantic the sea state is mostly duration-limited while it is usually closer to saturation in the low latitudes [*Bauer et al.*, 1999]. This is in correspondence to the logarithmic shape of the wave growth curve which shows that at full development the wave height is hardly influenced from changes of the wind duration. This also explains the rel-

atively large response obtained by *Cavaleri and Burgers* [1992] for fully developed seas when the contribution of the first effect is largest. However, another experiment with the WAM model and increased wind variability led to different results. If the wave model WAM is forced with an increased storm frequency in the North Atlantic by speeding up the flow of the weather then the mean wave heights and mean wave periods are reduced [*Bauer et al.*, 1999]. In the context of the present study the increased storm frequency may be regarded as a wind forcing which has a higher variability on scales of several hours than the original forcing. Increases of the wind variability on this time scales in the North Atlantic leads to a dominance of the effect of reduced wind duration over the effect causing increased wave growth. This resulted in a different overall effect than in the present study.

The sensitivity of the wave growth to high-frequency wind variability depends in an asymmetric manner on the excess of wind speed over the phase speed of the waves and on the characteristics of the waves themselves. Partly because the details of the physical process of wave generation are not known exactly the process is usually parameterized in wave models. In the wave model WAM the parameterization of the input source function is based on the theories of *Miles* [1957] and *Janssen* [1989]. Recently improved parameterizations of the wind input source function have been proposed [e.g., *Makin and Kudryavtsev*, 1999] which might improve the sensitivity to the wind variability in WAM. Since these parameterizations share the above mentioned asymmetry it is likely that the model response shows the same sign for these parameterizations but the actual size of the contributions and thus the variability may vary.

Another effect of the wave model response to high-frequency wind forcing is related to variations of the wind direction [*Ponce and Ocampo-Torres*, 1998]. In the present study this effect was neglected and we focused on the impact of high-frequency wind speed variations on the modeled wave field. Furthermore, also spatial correlations among the high-frequency wind fluctuations were neglected since they were not available from wind speed observations at a single platform. Such observations are now available from wind field observations of scatterometers on board of satellites. It has been shown already that for ocean circulation modeling the impact of such high-resolution wind vector data is advantageous [e.g., *Chen et al.*, 1999; *Kelly et al.*, 1999]. To gain more insight into the consequences of high-frequency fluctuations for the prediction of probability distributions of wave and ocean circulation data a further development of the wind generator presented in this study seems to be desirable and, in par-

ticalar, to incorporate the high-frequency directional wind variations and the spatial correlations of the wind fluctuations.

Acknowledgments. We are obliged to Jean Tournadre for providing us with the data from Frigg. The Ekofisk data were supplied by Loginfo A.S. The authors received funding from the European Union under ENV4-CT97-0460 (ASPEN) and from the BMBF project 03F0185A (KLINO).

References

- Bauer, E., H. von Storch, and M. Stolley, Sensitivity of ocean waves to speed changes of the weather stream, *Global Atmos. Ocean System*, in press, 1999.
- Bauer, E., Statistical comparison of winds from ERS-1 scatterometer and ECMWF model in time and wave number domain, *Proc. 3rd ERS Symp. on Space at the service of our environment, ESA SP-414*, 1195-1200, 1997.
- Bauer, E. and C. Staabs, Statistical properties of global significant wave heights and their use for validation, *J. Geophys. Res.*, 103, 1153-1166, 1998.
- Bürger, G., Expanded downscaling for generating local weather scenarios, *Clim. Res.*, 7, 111-128, 1996.
- Cavaleri, L., Wind variability. In: G.J. Komen, L. Cavaleri, M. Donelan, K. Hasselmann, S. Hasselmann, and P.A.E.M. Janssen, *Dynamics and Modelling of Ocean Waves*, Cambridge University Press, Cambridge, 320-331, 1994.
- Cavaleri, L., and G. Burgers, Wind gustiness and wave growth, *KNMI-Preprints, 92-18*, 38pp., Koninklijk Nederlands Meteorologisch Instituut, De Bilt, The Netherlands, 1992.
- Chen, D., W.T. Liu, S. Zebiak, M. Cane, Y. Yochanan and D. Witter, The sensitivity of the tropical Pacific Ocean simulation to the temporal and spatial resolution of wind forcing, *J. Geophys. Res.*, 104, 11,261-11272, 1999.
- Gibson, R., P. Kallberg, and S. Uppala, The ECMWF Re-Analysis (ERA) project, *ECMWF Newsletter*, 73, 7-17, 1996.
- Günther, H., and W. Rosenthal, A wave model with a non-linear dissipation function. In: 4th International workshop on wave hindcasting and forecasting, October 16-20, 1995, Banff, Alberta, Canada, pp. 138-147, 1995.
- Hasselmann, K., On the spectral dissipation of ocean waves due to white capping. *Boundary Layer Meteorol.* 6, 107-127, 1974.
- Hasselmann, S., and K. Hasselmann, Computations and parameterizations of the nonlinear energy transfer in a gravity-wave spectrum, part 1: A new method for efficient computations of the exact nonlinear transfer integral. *J. Phys. Oceanogr.* 15, 1369-1377, 1985.
- Hasselmann, S., K. Hasselmann, J.H. Allender, and T.P. Barnett, Computations and parameterizations of the nonlinear energy transfer in a gravity-wave spectrum, part 2: Parameterization of the nonlinear energy transfer for application in wave models. *J. Phys. Oceanogr.* 15, 1378-1391, 1985.
- Heimbach, P., S. Hasselmann and K. Hasselmann, Statistical analysis and WAM model intercomparison of wave spectral retrievals for a 3 year period of global ERS-1 SAR wave mode, *J. Geophys. Res.*, 103, 7931-7978, 1998.
- Janssen, P. A. E. M., Wave-induced stress and the drag of air flow over sea waves, *J. Phys. Oceanogr.*, 19, 745-754, 1989.
- Janssen, P. A. E. M., Quasi-linear theory of wind generation applied to wave forecasting, *J. Phys. Oceanogr.*, 22, 1600-1604, 1991.
- Komen, G.J., L. Cavaleri, M. Donelan, K. Hasselmann, S. Hasselmann, and P.A.E.M. Janssen, *Dynamics and Modelling of Ocean Waves*, Cambridge University Press, Cambridge, 532pp, 1994.
- Kelly, K.A., S. Dickinson and Z.J. Yu, NSCAT tropical wind stress maps: Implications for improving ocean modeling, *J. Geophys. Res.*, 104, 11,291-11,310, 1999.
- Makin, V.K. and V.N. Kudryavtsev, Coupled sea surface- atmospheric model, part 1, wind over wave coupling, *J. Geophys. Res.*, 104, 7613-7624, 1999.
- Miles, J. W., On the generation of surface waves by shear flows, *J. Fluid Mech.*, 3, 185-204, 1957.
- Monaldo, F., Corrected spectra of wind speed and significant wave height, *J. Geophys. Res.*, 95, 3399-3402, 1990.
- Ponce, S., and F. J. Ocampo-Torres, Sensitivity of a wave model to wind variability, *J. Geophys. Res.*, 103, 3179-3201, 1998.
- Schneggenburger, C., H. Günther, and W. Rosenthal, A shallow water wave model with nonlinear dissipation, *Dt. Hydrogr. Zeitschr.*, 49, 431-444, 1997.
- Sterl, A., G.J. Komen, and P.D. Cotton, Fifteen years of global wave hindcasts using winds from the European Centre for Medium-Range Weather Forecasts reanalysis: Validating the reanalyzed winds and assessing wave climate, *J. Geophys. Res.*, 103, 5477-5492, 1998.
- Tournadre, J., Time and space scales of significant wave heights, *J. Geophys. Res.*, 98, 4727-4738, 1993.
- Tournadre, J., B. Chapron, and D. Vandemark, Space scale analysis of wind speed and significant wave height, in *The air-sea interface, radio and acoustic sensing, turbulence and wave dynamics*, Eds.: M.A. Donelan, W.H. Hui, and W.J. Plant, pp. 629-634, Rosenstiel School of Mar. Atmos. Sci., 1996.
- von Storch, H., F.W. Zwiers, *Statistical analysis in climate research*, Cambridge University Press, 528 pp, in press, 1999.
- WAMDI Group, The WAM model - a third generation ocean wave prediction model, *J. Phys. Oceanogr.*, 18, 1775-1810, 1988.
- E. Bauer, Potsdam-Institut für Klimafolgenforschung, Telegrafenberg, P.O. Box 601203, D-14412 Potsdam, Germany. (bauer@pik-potsdam.de)
- R. Weisse, GKSS-Forschungszentrum Geesthacht, Institut für Gewässerphysik, Max-Planck-Straße 1, D-21502 Geesthacht, Germany. (weisse@gkss.de)

Figure 1. (a) EOF 1 of the observed wind fluctuations. The x-axis represents the time within a 6 hour time slot. The fluctuations are denoted by u' . (b) Lagged auto correlation function of the related coefficient time series. Here the x-axis denotes consecutive 6 hour intervals. The 95% confidence interval is indicated by the dashed line. (c) Quantile-Quantile plot of the standard normal distribution and the probit transformed first EOF coefficient time series. The 99% confidence interval is indicated by the two thin solid lines.

Figure 2. Frequency spectra of the wind speed measured at Ekofisk from time series with 20 min temporal resolution. Units are $\text{m s}^{-2} \times 20 \text{ min}$. The spectra are shown from the original measurements (solid line), the linearly interpolated 6 hour measurements (solid with dots), and the linearly interpolated 6 hour measurements with superimposed high-frequency fluctuations from the wind generator (dashed). The spectral slope of $f^{-1.7}$ is indicated by the straight line. The error bar shows the 95% confidence interval.

Figure 3. (a) Frequency spectra of significant wave heights at Frigg obtained from time series with 20 min temporal resolution. Units are $\text{m}^2 \times 20 \text{ min}$. The spectra are shown from the original measurements (solid line), the CTR experiment (solid with dots), the HF1 experiment (dashed), and the HF3 experiment (dashed-dotted). The spectral slope of $f^{-1.7}$ is indicated by the straight line. The error bar shows the 95% confidence interval. (b) Ratio of spectral variance of wind speed of the HF1 (solid) and the HF3 experiment (dashed) relative to CTR experiment. (c) Ratio of spectral variance of significant wave height of the HF1 (solid) and the HF3 experiment (dashed) relative to CTR experiment.

Figure 4. Differences of mean SWH in cm between the HF1 and the CTR experiment. The areas A and B are marked with bold solid lines. For the definition of these areas see text.

Figure 5. Differences of quantiles between the HF1 and the CTR experiment for the areas A (storm track, solid lines) and B (outside the storm track, dashed line). (a) friction velocity in m s^{-1} ; (b) coupling ratio; (c) significant wave height in m; (d) mean frequency in Hz. For the definition of the areas see Figure 4.

Figure 6. Cumulative frequency distribution of the instantaneous differences of SWH between the HF1 and the CTR experiment for areas A (storm track, solid line) and B (outside the storm track, dashed line) relative to the mean SWH of that area. For the definition of the areas see Figure 4.

Table 1. The first three moments (mean, standard deviation and skewness) of u_{10} and SWH at Frigg as obtained from the three model experiments and the observations. For wind speed the moments were computed for the period 1 October 1983 until 31 March 1984 (upper 4 rows), for SWH the moments were computed for the period from 1 January 1984 until 31 March 1984 (lower 4 rows). Periods containing data gaps in the observations were excluded from all computations and number of samples are indicated by N .

	CTR	HF1	HF3	Frigg
N	11219	11219	11219	11219
mean [m/s]	10.6	10.6	10.7	9.6
std [m/s]	4.14	4.31	4.65	4.20
skewness	0.087	0.088	0.119	0.091
N	6219	6219	6219	6219
mean [m]	3.6	3.7	3.8	3.3
std [m]	1.67	1.67	1.68	1.46
skewness	0.857	0.863	0.900	0.461

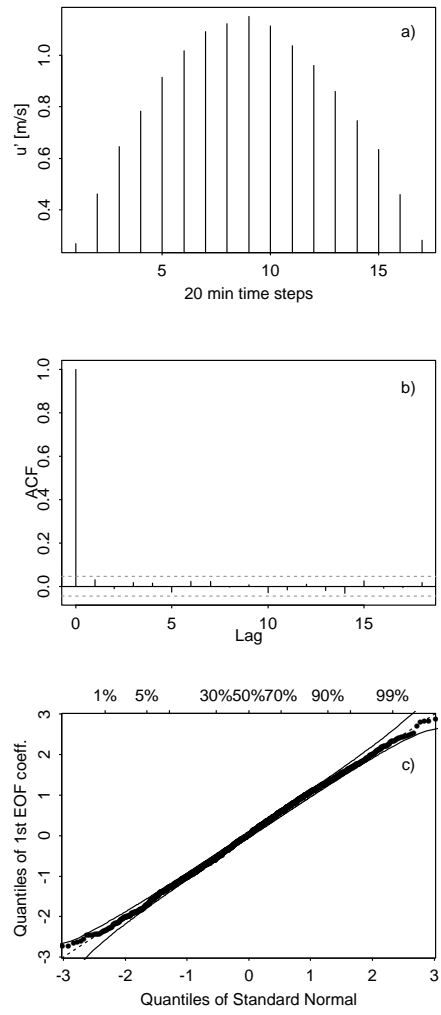


Figure 1. (a) EOF 1 of the observed wind fluctuations. The x-axis represents the time within a 6 hour time slot. The fluctuations are denoted by u' . (b) Lagged auto correlation function of the related coefficient time series. Here the x-axis denotes consecutive 6 hour intervals. The 95% confidence interval is indicated by the dashed line. (c) Quantile-Quantile plot of the standard normal distribution and the probit transformed first EOF coefficient time series. The 99% confidence interval is indicated by the two thin solid lines.

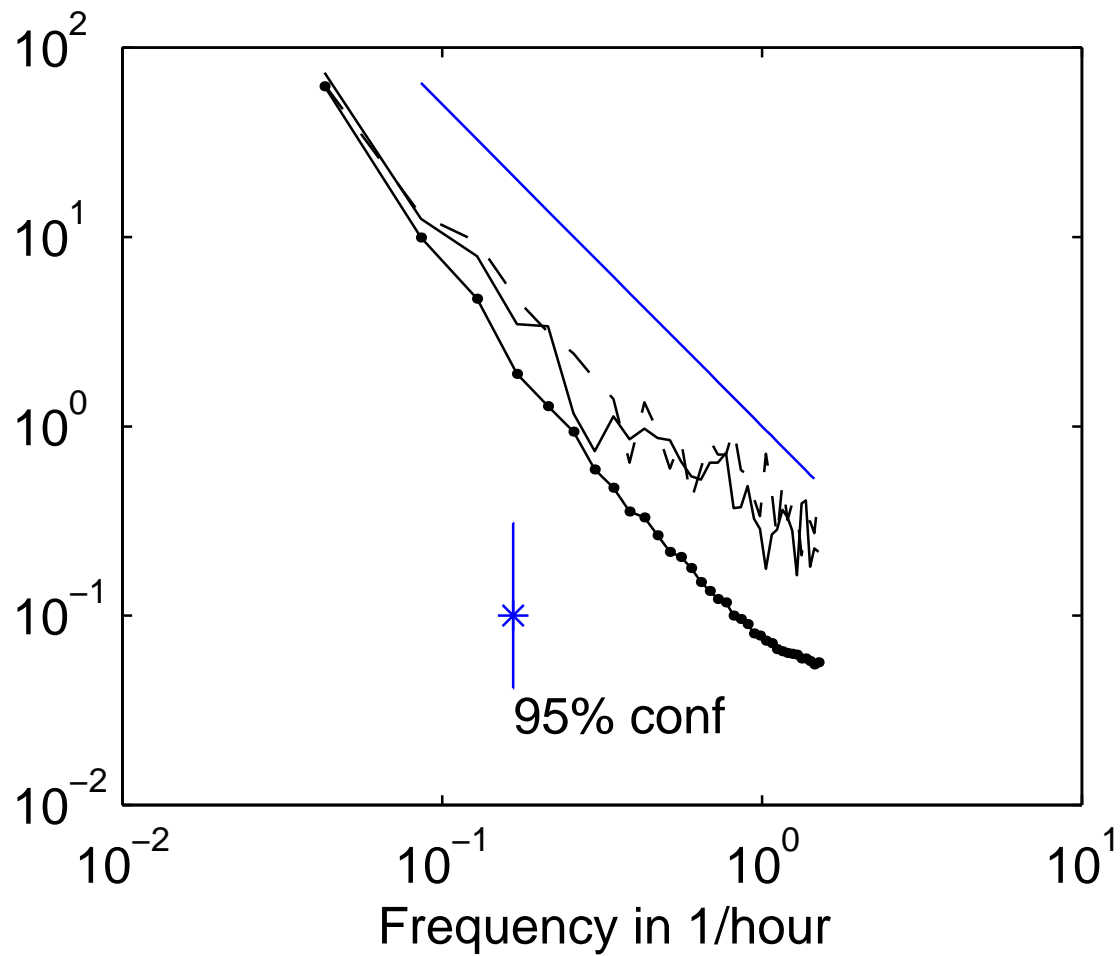


Figure 2. Frequency spectra of the wind speed measured at Ekofisk from time series with 20 min temporal resolution. Units are $\text{m s}^{-2} \times 20 \text{ min}$. The spectra are shown from the original measurements (solid line), the linearly interpolated 6 hour measurements (solid with dots), and the linearly interpolated 6 hour measurements with superimposed high-frequency fluctuations from the wind generator (dashed). The spectral slope of $f^{-1.7}$ is indicated by the straight line. The error bar shows the 95% confidence interval.

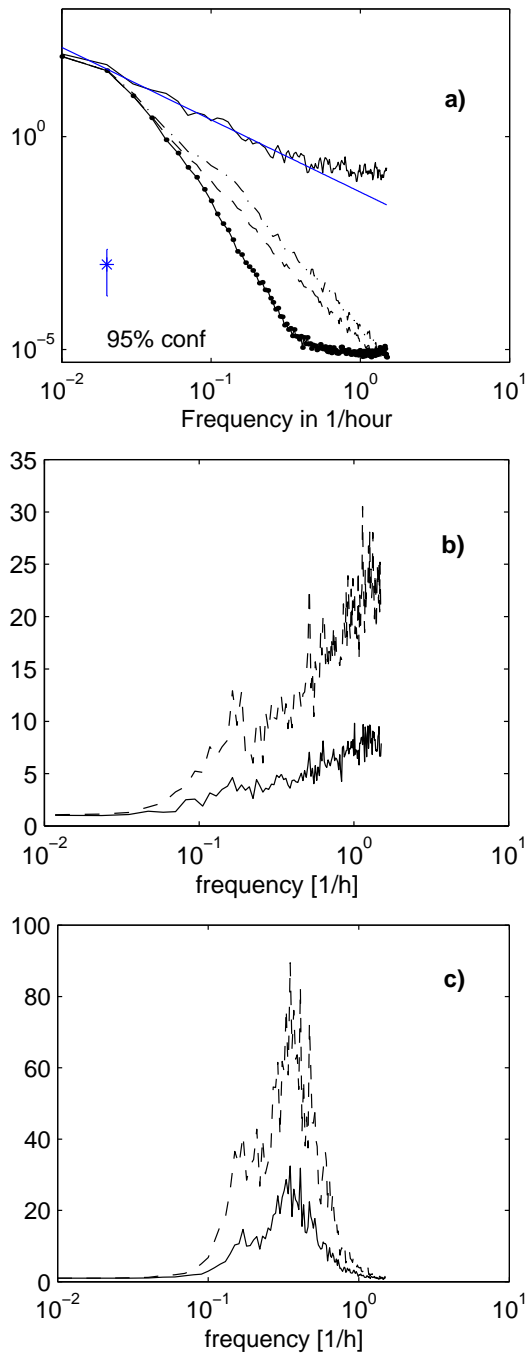


Figure 3. (a) Frequency spectra of significant wave heights at Frigg obtained from time series with 20 min temporal resolution. Units are $m^2 \times 20 \text{ min}$. The spectra are shown from the original measurements (solid line), the CTR experiment (solid with dots), the HF1 experiment (dashed), and the HF3 experiment (dashed-dotted). The spectral slope of $f^{-1.7}$ is indicated by the straight line. The error bar shows the 95% confidence interval. (b) Ratio of spectral variance of wind speed of the HF1 (solid) and the HF3 experiment (dashed) relative to CTR experiment. (c) Ratio of spectral variance of significant wave height of the HF1 (solid) and the HF3 experiment (dashed) relative to CTR experiment.

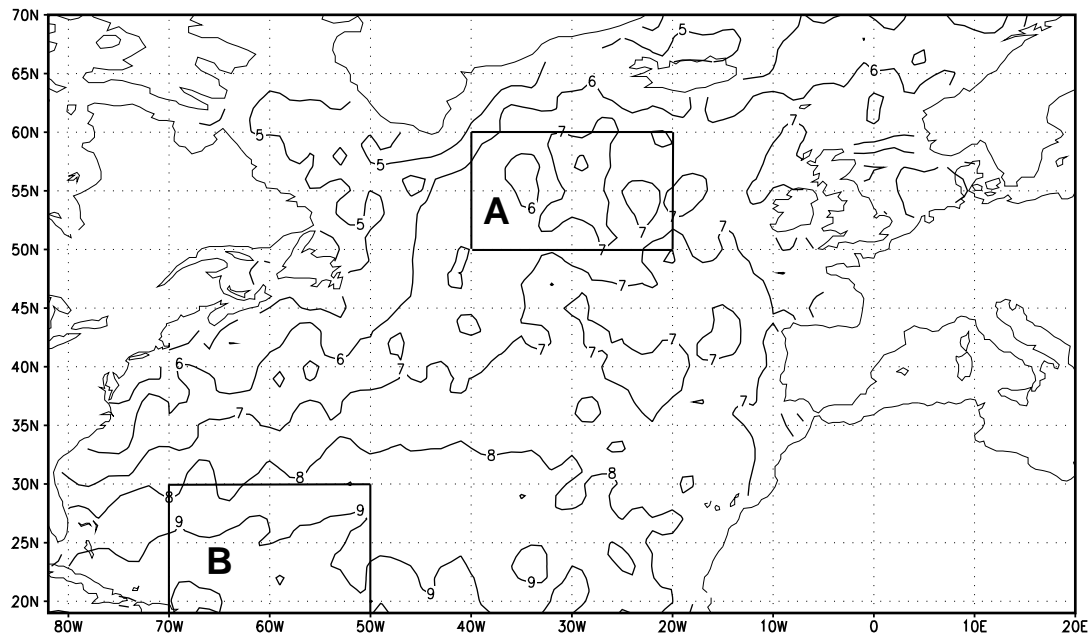


Figure 4. Differences of mean SWH in cm between the HF1 and the CTR experiment. The areas A and B are marked with bold solid lines. For the definition of these areas see text.

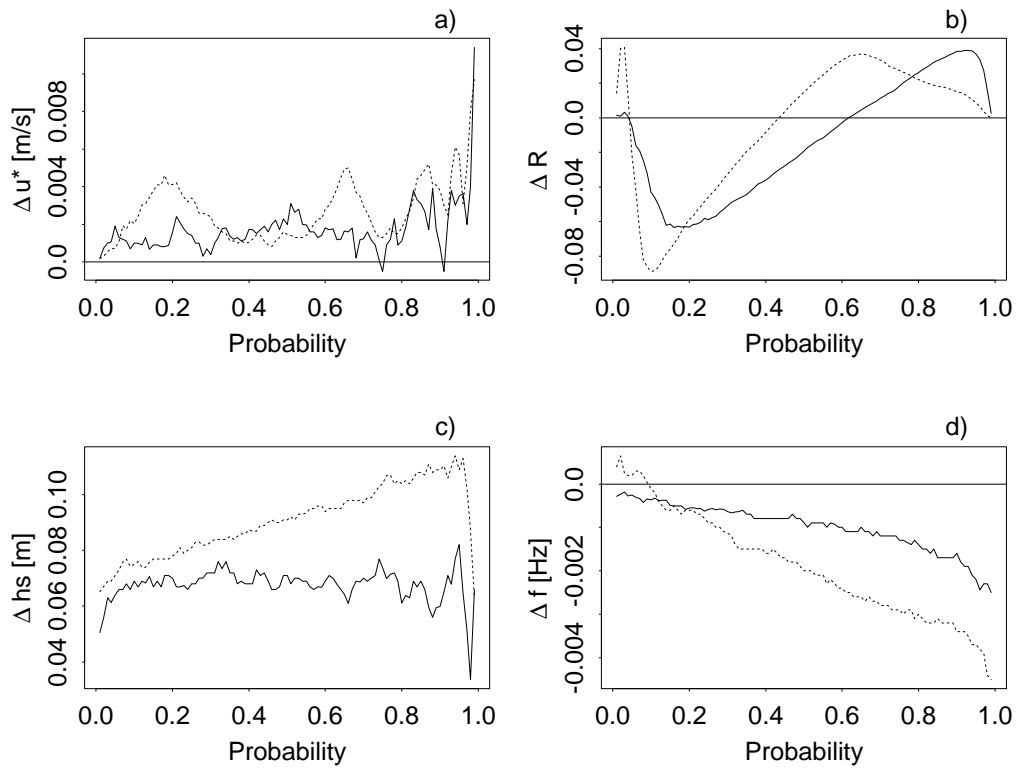


Figure 5. Differences of quantiles between the HF1 and the CTR experiment for the areas A (storm track, solid lines) and B (outside the storm track, dashed line). (a) friction velocity in m s^{-1} ; (b) coupling ratio; (c) significant wave height in m; (d) mean frequency in Hz. For the definition of the areas see Figure 4.

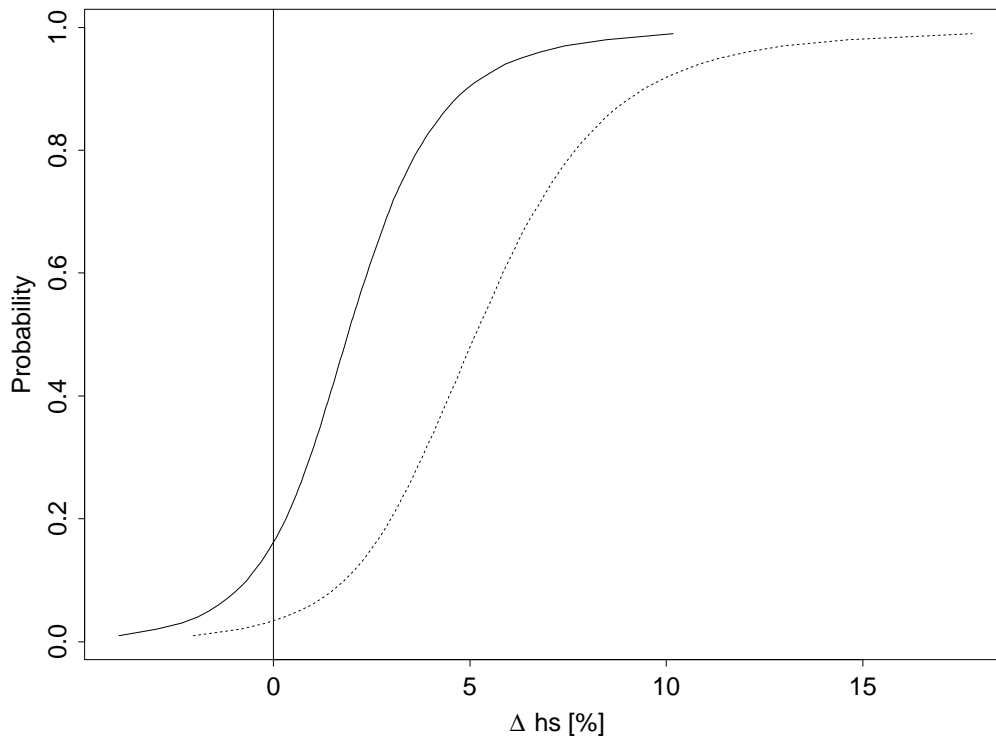


Figure 6. Cumulative frequency distribution of the instantaneous differences of SWH between the HF1 and the CTR experiment for areas A (storm track, solid line) and B (outside the storm track, dashed line) relative to the mean SWH of that area. For the definition of the areas see Figure 4.